Missouri University of Science and Technology
Scholars' Mine

Nuclear Engineering and Radiation Science Faculty Research & Creative Works

Nuclear Engineering and Radiation Science

28 Sep 2021

Vacancy-Induced Enhancement of Electron-Phonon Coupling in Cubic Silicon Carbide and its Relationship to the Two-Temperature Model

Salah Al Smairat

Joseph T. Graham
Missouri University of Science and Technology, grahamjose@mst.edu

Follow this and additional works at: https://scholarsmine.mst.edu/nuclear_facwork

Part of the Nuclear Engineering Commons

Recommended Citation

S. Al Smairat and J. T. Graham, "Vacancy-Induced Enhancement of Electron-Phonon Coupling in Cubic Silicon Carbide and its Relationship to the Two-Temperature Model," *Journal of Applied Physics*, vol. 130, no. 12, article no. 125902, American Institute of Physics (AIP), Sep 2021.
The definitive version is available at https://doi.org/10.1063/5.0056244

This Article - Journal is brought to you for free and open access by Scholars' Mine. It has been accepted for inclusion in Nuclear Engineering and Radiation Science Faculty Research & Creative Works by an authorized administrator of Scholars' Mine. This work is protected by U. S. Copyright Law. Unauthorized use including reproduction for redistribution requires the permission of the copyright holder. For more information, please contact scholarsmine@mst.edu.

Journal of Applied Physics | ARTICLE | scitation.org/journal/jap

Vacancy-induced enhancement of electron–phonon coupling in cubic silicon carbide and its relationship to the two-temperature model

Cite as: J. Appl. Phys. **130**, 125902 (2021); doi: 10.1063/5.0056244
Submitted: 7 May 2021 · Accepted: 2 September 2021 ·
Published Online: 27 September 2021

Salah Al Smairat and Joseph Graham[a)]

AFFILIATIONS

Department of Nuclear Engineering and Radiation Science, Missouri University of Science and Technology, Rolla, Missouri 65409, USA

[a)]**Author to whom correspondence should be addressed:** grahamjose@mst.edu

ABSTRACT

The electron–phonon coupling factor was calculated for both pristine and vacancy-rich 3C-SiC. *Ab initio* calculations were performed within the framework of the density functional perturbation theory. Wannier functions were used to interpolate eigenvalues into denser grids through the electron–phonon using Wannier code. The coupling factor was determined through calculations of the electron self-energy, electron–phonon relaxation time, and electronic specific heat. These parameters were extrapolated to high temperatures using a hybrid model which mixes band calculations for electrons below an energy cutoff with the free electron gas model for electrons above the energy cutoff. The electron relaxation times, specific heats, electron drift mobilities, and electron–phonon coupling factors were calculated as a function of electron temperature. Si and C vacancies were found to have a profound effect on electron–phonon coupling for all temperatures, while electronic specific heat capacity was found to be most affected at cryogenic temperatures. The electron drift mobility was calculated at different temperatures using the scattering time. Calculated mobilities were validated with Hall mobility measurements reported in the literature. The importance of structural defects on the electron–phonon coupling is discussed in the context of the two-temperature model, a model that has been widely used to understand aspects of the interaction of solids with pulsed laser irradiation and swift heavy ion irradiation.

Published under an exclusive license by AIP Publishing. https://doi.org/10.1063/5.0056244

I. INTRODUCTION

Silicon carbide is a high-temperature ceramic with numerous commercial and industrial uses. Its utility arises from a combination of desirable properties such as high hardness, high thermal conductivity, low coefficient of thermal expansion, semiconducting properties, and radiation tolerance.[1,2] In the nuclear power industry, SiC is used in high-temperature gas-cooled reactors as a coating in tri-isostructural (TRISO) fuel particles. It is also being considered for use as a cladding material in light water reactors[1,3] and as a structural material in the flow channels of fusion systems.[4]

Materials in nuclear energy systems are exposed to intense fields of neutrons, gamma rays, and fission products. The interaction of radiation with matter results in the transfer of energy from incident particles to the lattice through nuclear energy loss and to electrons through electronic energy loss.[5] The former can produce structural disorder through the introduction of elementary point defects such as vacancies and self-interstitials. Higher-order defects such as clusters, dislocations, and voids can subsequently form and grow.[6] Electronic energy loss describes the excitation of the electronic structure and the generation of delta electrons. Energy transfer from the electronic system to the lattice is mediated, to a large extent, by electron–phonon coupling,[7] though in semiconductors, trap-assisted radiative and non-radiative recombination processes are also important.[8] Understanding electron–phonon coupling in the presence of structural defects and as a function of electron temperature is an important element in developing a complete picture of radiation interactions and radiation effects when both nuclear and electronic energy loss mechanisms are present. In SiC, an interesting competitive relationship between nuclear and electronic energy loss was recently observed.[9] Structural disorder produced in SiC with ions in the nuclear energy loss regime was found to be partially annealed upon irradiation with ions in the electronic

Published under an exclusive license by AIP Publishing

energy loss regime. Reasons for this may stem from modulation of the electron–phonon coupling and thermal diffusivity via defects. This paper examines the former.

The electron–phonon interaction is also an important quasi-particle interaction that modifies both the electron and phonon self-energies in a material. It is, therefore, connected to the basic thermodynamic and transport properties of the material.[10] The electron–phonon coupling factor discussed in this work is the dimensionful factor appearing in the two-temperature model, a model that has been used to describe the transfer of energy from hot electrons to a lattice.[11,12] The two-temperature model is expressed through the following equations:

$$C_e \frac{\partial T_e}{\partial t} = \nabla \cdot [k_e \nabla T_e] - G(T_e - T_{ph}) + A(\boldsymbol{r}, t), \quad (1)$$

$$C_{ph} \frac{\partial T_{ph}}{\partial t} = \nabla \cdot [k_{ph}\ \nabla T_{ph}] + G(T_e - T_{ph}), \quad (2)$$

where $A(\boldsymbol{r}, t)$ represents the space- and time-dependent energy source (e.g., pulsed laser or swift charged particle), C_e ° and C_{ph} are the specific heat capacities of electrons and the lattice, respectively, k_e and k_{ph} are the corresponding thermal conductivities for electrons and the lattice, and T_e and T_{ph} are the temperatures of the electrons and the lattice, respectively. In the two-temperature model, it is assumed that electrons and the lattice are at quasi-thermodynamic equilibrium, which is to say that energy is rapidly shared among electrons establishing a well-defined local electron temperature, and energy is efficiently shared among phonons establishing a well-defined local lattice temperature. The two temperatures can be different owing to the slow transfer of energy from electrons to lattice. The rate of energy transfer is governed by $G(T_e - T_{ph})$.

Various approaches for determining G have been made. Here, we follow the approach of Ref. 13, which takes as the value of G,

$$G = \frac{C_e}{\tau}, \quad (3)$$

where τ is the electron–phonon relaxation time (inverse scattering rate). It should be mentioned that the *dimensionless* electron–phonon coupling constant—which frequently appears in the context of superconductivity in metals—can also be related to the dimensionful factor.[14,15] Though well-defined for metals at cryogenic temperatures, the dimensionless constant presupposes that only electron scattering at the Fermi surface contributes to energy transfer.[7] In bandgap materials, electron–phonon scattering occurs in the conduction and valence bands. Therefore, the factor discussed from this point forth pertains only to the definition in Eq. (3).

The main goal of this study is to understand the effect of Si and C vacancies on electron–phonon coupling in cubic SiC. Using the density functional perturbation theory (DFPT), the electron–phonon coupling factors and conduction electron lifetimes were calculated in pristine 3C-SiC and in relaxed supercells of 3C-SiC containing Si or C vacancies. The model was validated through the comparison of predicted electron drift mobilities and electron Hall mobility measurements, reported in the literature.

II. THEORY AND METHODOLOGY

A. The electron relaxation time

The electron relaxation time is related to the imaginary part of the electron self-energy, $\sum_{nk}$ (with band n and wave vector $\boldsymbol{k}$). In the Migdal approximation, the mode-resolved scattering rates (inverse relaxation times) are given by[16]

$$\frac{1}{\tau_{nk}} = 2\mathrm{Im}\sum_{nk} = \frac{2\pi}{\hbar}\sum_{mv}\int \frac{d\boldsymbol{q}}{\Omega_{BZ}} |g^{v}_{mn}(\boldsymbol{k}, \boldsymbol{q})|^2 [(1 - f_{m\boldsymbol{k}+\boldsymbol{q}} + n_{\boldsymbol{q}v}) \times \delta(\varepsilon_{n\boldsymbol{k}} - \varepsilon_{m\boldsymbol{k}+\boldsymbol{q}} - \hbar\omega_{\boldsymbol{q}v}) + (f_{m\boldsymbol{k}+\boldsymbol{q}} + n_{\boldsymbol{q}v})\delta(\varepsilon_{n\boldsymbol{k}} - \varepsilon_{m\boldsymbol{k}+\boldsymbol{q}} + \hbar\omega_{\boldsymbol{q}v})], \quad (4)$$

where $g^{v}_{mn}(\boldsymbol{k}, \boldsymbol{q})$ are the electron–phonon matrix elements,

$$g^{v}_{mn}(\boldsymbol{k}, \boldsymbol{q}) = \left\langle \psi_{m\boldsymbol{k}+\boldsymbol{q}} | \partial_{\boldsymbol{q}v} V | \psi_{n\boldsymbol{k}} \right\rangle. \quad (5)$$

Here, $\partial_{\boldsymbol{q}v} V$ is the partial derivative of the effective potential with respect to the lattice normal mode indexed by wave vector $\boldsymbol{q}$ and branch v. Each electron–phonon matrix element represents the transition amplitude for an electron in state $\psi_{n\boldsymbol{k}}$ (with wave vector $\boldsymbol{k}$ and branch n) to scatter into state $\psi_{m\boldsymbol{k}+\boldsymbol{q}}$ due to the perturbation in the effective potential resulting from atomic motion. $f_{m\boldsymbol{k}+\boldsymbol{q}}$ are the Fermi occupation numbers for electrons and $n_{\boldsymbol{q}v}$ are the Bose occupation numbers for phonons. It is here assumed that the electron and phonon occupation numbers are calculated at different temperatures. $\varepsilon_{n\boldsymbol{k}}$ and $\hbar\omega_{\boldsymbol{q}v}$ are electron and phonon energies, respectively. The integral is performed over the first Brillouin zone, which has volume Ω_{BZ}.

B. Calculation of matrix elements

Density functional perturbation theory (DFPT) calculations were performed on $2\times2\times2$ supercells of 3C-SiC. After relaxing the atomic coordinates to minimize total energy, ground state wave functions were calculated on a uniform $6\times6\times6$ k-grid with a cutoff energy of 60 Ry using the Quantum Espresso code.[17] Phonon frequencies and polarization vectors were calculated on a uniform $3\times3\times3$ q-grid centered at Γ using the perturbation theory method. The resulting polarization vectors were used to deform the effective potential along phonon normal coordinates, taking $V \rightarrow V + \partial_{\boldsymbol{q}v} V$. The matrix elements were then determined by taking the product of the in and out Bloch states with the perturbing potential [Eq. (5)].

The resulting matrix elements were Wannierized and interpolated onto a $12\times12\times12$ k-grid and $46\times46\times46$ q-grid using the Electron–Phonon using Wannier (EPW) code.[18,19] The density of the k-point grid was increased until the maximum differences in the imaginary electron self-energy converged to within 5%. This resulted in a final interpolated grid of $12\times12\times12$ for the k-point grid and $46\times46\times46$ for the q-point grid. EPW was subsequently used to determine the electron self-energies and relaxation times. Calculations in defective supercells of SiC were performed by adding a single C or Si vacancy into the supercell and relaxing the structure. This corresponded to C or Si vacancy concentrations of 12.5%. Those defective supercells will hereafter be referred to as

Published under an exclusive license by AIP Publishing

$SiC_{0.875}$ or $Si_{0.875}C$. Initial projections used sp^3 hybridized orbitals for the pristine cell and random projections for the defective cells.

Relaxation times were calculated from 20 to 10^6 K. In order to parameterize the relaxation time as a function of electron temperature, several simplifying assumptions were made. The electron temperature dependence appears through the Fermi occupation numbers in Eq. (4). The use of Fermi–Dirac statistics for the electron system assumes that the hot electrons and holes have established quasi-thermal equilibrium, which is to say that they can be characterized by a single electron temperature. In the context of the two-temperature model, where a rapid excitation source is present, such an assumption is likely only valid after an initial equilibration period has elapsed and provided that the electron–electron interaction rate is significantly greater than the electron–phonon scattering rate. Alternative approaches might also consider using quasi-Fermi levels for both electrons and holes or using Boltzmann transport or Monte Carlo methods to study the non-equilibrium dynamics. However, in the context of the two-temperature model, it is necessary to parameterize all material properties by a single electron temperature and single lattice temperature.

C. Hybrid model of specific capacity and the electron–phonon coupling factor

At low and intermediate temperatures, the Fermi occupation numbers are negligibly small above the highest band energies, E_{max}, calculated using the DFT code (approximately 11 eV above the Fermi level). However, above about 10^5 K, the number of electrons above the highest energy bands begins to become non-negligible. The contribution of those high-energy electrons is approximated by treating them as a free electron gas obeying Boltzmann statistics. The use of Boltzmann statistics is justified as high-energy states are sparsely occupied. The hybrid electronic specific heat capacity is, therefore, made up of two parts,

$$C_e(T) = \frac{2}{N_k}\sum\nolimits_{nk} C_{nk} + \frac{3}{2}k_B n_{free}(T). \tag{6}$$

The first term is the heat capacity determined from the static band calculations. The second term is the specific heat capacity of a Maxwell–Boltzmann distributed gas of free electrons and is only important above 10^5 K. C_{nk} are the mode-resolved electronic heat capacities due to electrons in the calculated band structure, which has a maximum energy of E_{max},

$$C_{nk} = \frac{(\epsilon_{nk} - \epsilon_f)^2 \exp\left(\frac{\epsilon_{nk} - \epsilon_f}{k_B T}\right)}{k_B T^2\left[1 + \exp\left(\frac{\epsilon_{nk} - \epsilon_f}{k_B T}\right)\right]^2}, \tag{7}$$

where ϵ_f is the Fermi level and N_k is the number of sampled wave vectors in the Brillouin zone ($N_k = 1728$ for these calculations). The factor of 2 appearing before the first term in Eq. (6) accounts for electron spin. To connect Fermi–Dirac statistics for electrons below E_{max} with Boltzmann statistics above E_{max}, the following approximation is used for the product of the electronic density of states D and the Fermi–Dirac distribution f:

$$D(\epsilon)f(\epsilon - \epsilon_f; T) \cong \exp\left(-\frac{E_{max} - \epsilon_f}{k_B T}\right) \times \exp\left(-\frac{\epsilon - E_{max}}{k_B T}\right) D_{MB}(\epsilon - E_{max}), \tag{8}$$

where $\epsilon > E_{max}$ and D_{MB} is the density of states of a Maxwell–Boltzmann gas. Integrating Eq. (8) over energy gives the number of free electrons,

$$n_{free}(T) = \int_{E_{max}}^{\infty} D(\epsilon)f(\epsilon - \epsilon_f; T)d\epsilon = N\exp\left(-\frac{E_{max} - \epsilon_f}{k_B T}\right), \tag{9}$$

where N is the total number of valance electrons of SiC. For high temperatures, the Fermi level was adjusted to ensure the conservation of valence electrons. At temperatures below 10^4 K, no adjustment of the Fermi level was needed. While such a treatment of the high-energy electrons is highly approximate, it is necessary to account for their energy contributions in some way. Otherwise, the specific heat capacity will be unphysically low at high temperatures and may even decrease. Note that in this scheme, each valence electron in the structure has one valence state, one conduction/excited state, and one free particle state. Extending Eq. (3) and incorporating the contribution of free electrons to the electron–phonon coupling factor, one obtains

$$G = \frac{2}{N_k}\sum_{nk}\frac{C_{nk}}{\tau_{nk}} + \frac{3k_B n_{free}(T)}{2\tau_{free}(T)}. \tag{10}$$

The relaxation time for free electrons, $\tau_{free}(T)$, is approximated as follows. The scattering rate is given by

$$\frac{1}{\tau_{free}(T)} = \bar{\Sigma}\langle v\rangle. \tag{11}$$

Here, the mean cross section, $\bar{\Sigma}$, is assumed to be a sum of geometric cross sections for ionic cores,

$$\bar{\Sigma} = \rho_C\sigma_C + \rho_{Si}\sigma_{Si} = \rho_C(\pi r_c^2) + \rho_{Si}(\pi r_{Si}^2), \tag{12}$$

where ρ_C and ρ_{Si} are the number densities of carbon and silicon atoms and r_C and r_{Si} are the ionic radii. The mean velocity of the free electrons, $\langle v\rangle$, which is also the mean velocity of a Maxwell–Boltzmann gas is

$$\langle v\rangle = \sqrt{\frac{8k_B T}{\pi m_e}}, \tag{13}$$

where m_e is the electron mass.

Published under an exclusive license by AIP Publishing

D. Electron mobilities and the electron–phonon mean free path

In order to validate these first principles calculations with experimental data, the electron drift mobilities were calculated and compared to experimentally measured electron Hall mobilities in donor-doped 3C-SiC. The electron drift mobility can be obtained from the conduction electron relaxation time using

$$\mu_e = \frac{e\tau}{m_e^*}, \tag{14}$$

where τ is the thermal-averaged conduction electron relaxation time and m_e^* is the effective mass of the electrons. μ_e is measured by applying a magnetic field perpendicular to the carrier currents that are induced by an electromotive force. This, in turn, produces a potential difference, the Hall voltage V_H,[20] which can be measured and used to extract the Hall mobilities for electrons and holes. The electron mobility was calculated using

$$\mu_e = \frac{e}{m_e^*}\frac{\sum_{CB,\mathbf{k}} \tau_{n\mathbf{k}} f(\epsilon_{n\mathbf{k}} - \epsilon_f;\, T)}{\sum_{CB,\mathbf{k}} f(\epsilon_{n\mathbf{k}} - \epsilon_f;\, T)}. \tag{15}$$

The quotient of the sums gives the thermal-averaged relaxation time. The sums run over the lowest conduction band only. Near 0 K, the average relaxation time approaches the relaxation time at the conduction band minimum (CBM) (bottom of the X valley). Mobilities were calculated up to 1000 K. In that temperature range, higher energy conduction bands and the free electron states could be ignored. The value of m_e^* used was the effective Hall mass $m_e^* = 0.67 m_e$.[21]

The average mean free path of electrons was also calculated from the relaxation time using

$$\lambda_{n\mathbf{k}} = |v_{g,n\mathbf{k}}|\tau_{n\mathbf{k}}, \tag{16}$$

where $v_{g,n\mathbf{k}}$ are the electron group velocities. These mean free path values were used to assess the degree of localization in the electron–phonon interaction.

III. RESULTS AND DISCUSSION

A. Phonon density of states

The calculated phonon dispersion curves of the pristine lattice using a $6 \times 6 \times 6$ q-grid are displayed in Fig. 1. SiC has two atoms per primitive unit cell, corresponding to six phonon modes, three of which are acoustic modes and three of which are optical modes. The electron–phonon interaction depends strongly on the polarization of the phonon modes. For example, the matrix elements of the transverse acoustic (TA) modes are smaller than the longitudinal acoustic (LA) mode because the LA mode produces both shear strain and volume dilation/contraction, while TA modes produce only shear strain.[22]

The calculated phonon dispersion curves are in good agreement with inelastic x-ray scattering[23] and Raman scattering[24] measurements. The phonon density of states (DOS) of the pristine lattice using a $6 \times 6 \times 6$ q-grid is shown in Fig. 2. The high-frequency peaks are mainly associated with vibrations of the lighter carbon atoms,

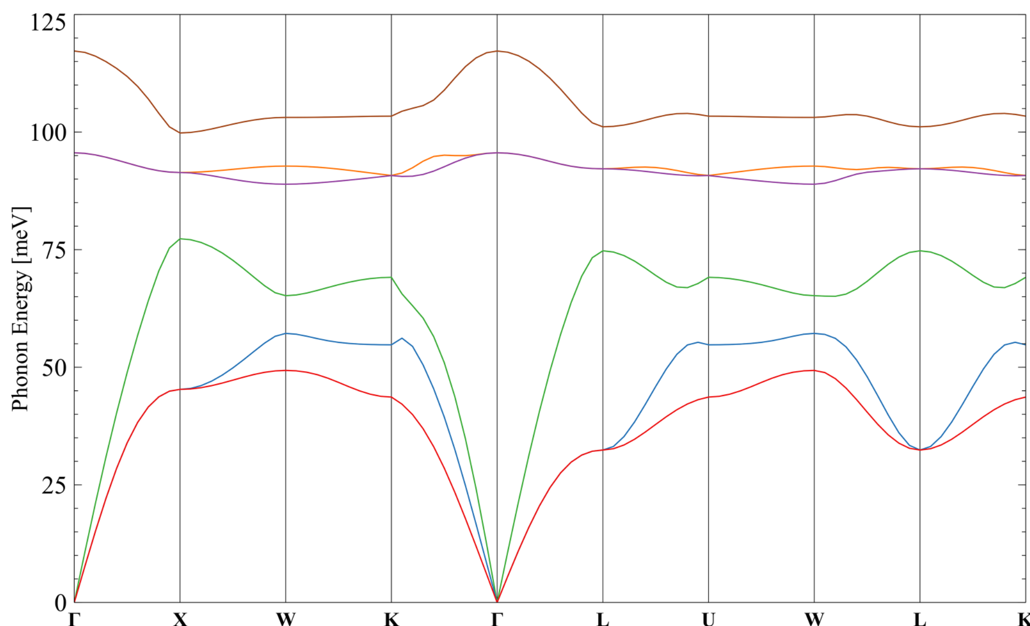

FIG. 1. Phonon dispersion curves of pristine 3C-SiC lattice calculated on a 6 × 6 × 6 coarse q-grid.

Published under an exclusive license by AIP Publishing

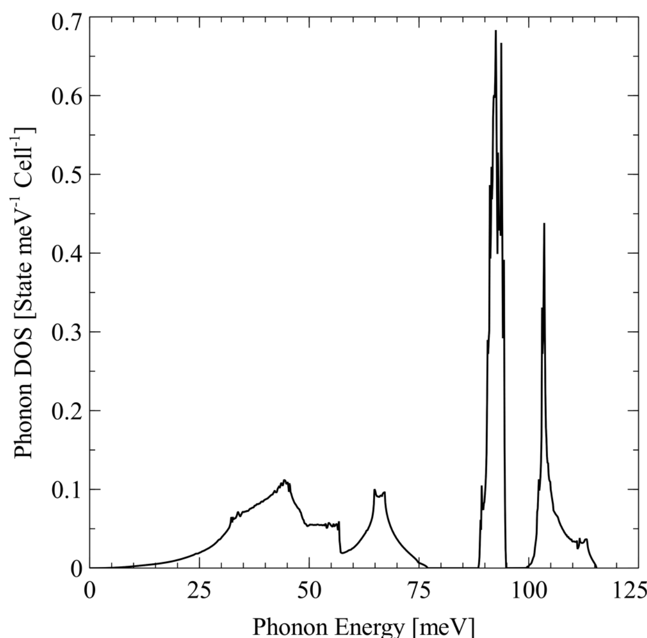

FIG. 2. Phonon density of states of the pristine 3C-SiC lattice calculated on a 6 × 6 × 6 coarse q-grid.

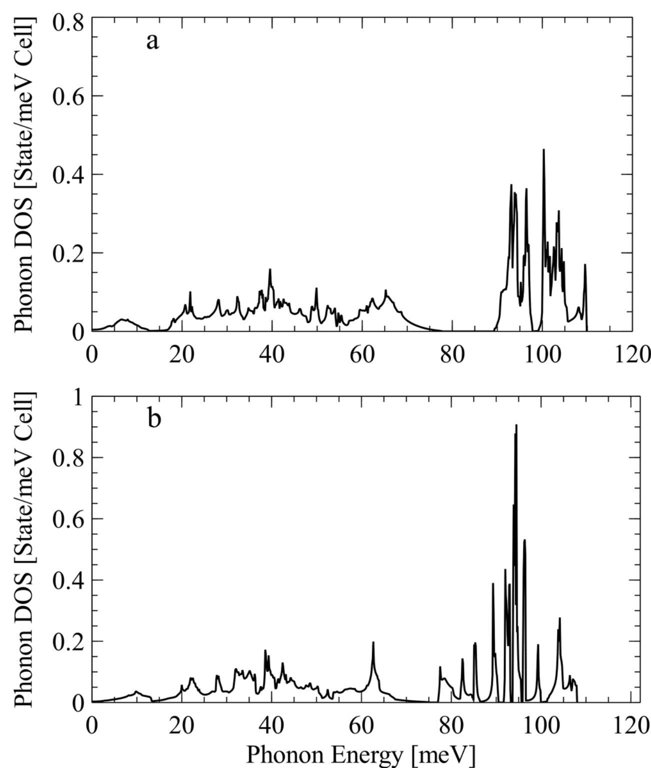

FIG. 3. (a) Phonon DOS of $Si_{0.875}C$ and (b) phonon DOS of $SiC_{0.875}$. Modes were interpolated onto a 12 × 12 × 12 coarse q-grid.

while the lower frequency features tend to have a more mixed character.

The effect of vacancies on the phonon DOS is illustrated in Fig. 3. Both vacancy types cause splitting and the appearance of low energy modes. This is expected from the interruption of long-range order and a decrease in the average Si–C bond strength. In $SiC_{0.875}$, there is a greater degree of splitting and a notable down shift in the energies of the optical phonons which is expected as those phonon branches are largely characterized by vibrations on the carbon sublattice.

B. Electron band structure

The electron band structure for pristine 3C-SiC is shown in Fig. 4. The corresponding electron DOS is shown in Fig. 5. These results show good agreement with the computational literature[25] and experimental literature.[26] Figure 6 shows the electron DOS for $Si_{0.875}C$ and $SiC_{0.875}$.

C. Electron–phonon relaxation times and G

Referring to Fig. 4, the upper three valance bands (bands 2, 3, and 4) meet at the valence band maximum (VBM) while the conduction band minimum (CBM) occurs in only the lowest conduction band (band 5). Therefore, at low temperatures, those four bands have the greatest contribution to the specific heat capacity, electron–phonon coupling factor, and electron mobility. Relaxation times are plotted along a Brillouin zone path in Fig. 7. The three upper valence bands are shown by the dashed red lines, while the lowest conduction band is shown by the dotted blue line.

As expected, the relaxation time of the lowest conduction band is highest at X due to the valley at that point (X valley). The maximum relaxation time for valence electrons occurs at Γ, coinciding with the valence band maximum.

The relaxation times for pristine 3C-SiC are plotted in Fig. 8 as a function of the difference in energy between the electron energy level and the Fermi level.

As with Fig. 7, the longest lived carriers are found at the VBM and the CBM. The CBM electrons lack lower energy states to scatter into. Similarly, holes in the VBM lack higher energy states to scatter into. Meanwhile, in the middle of the bands, the abundance of adjacent states reduces the lifetime to around 10^{-14} s. The relaxation times also decrease as temperature increases due to the lowering of occupation numbers.

The situation changes when vacancies are added. The narrowing of the bandgap and production of in-gap defect states increase the number of states that conduction electrons near the band edge can scatter down into and valence band holes can scatter up into. Figure 9(a) shows how the lifetimes of states near the VBM and CBM decrease by several orders of magnitude due to the narrowing of the bandgap in $Si_{0.875}C$ (Fig. 6). States near the VBM are particularly affected. Figure 9(b), which shows the same for $SiC_{0.875}$, indicates a less pronounced change in the relaxation time near the VBM.

Published under an exclusive license by AIP Publishing

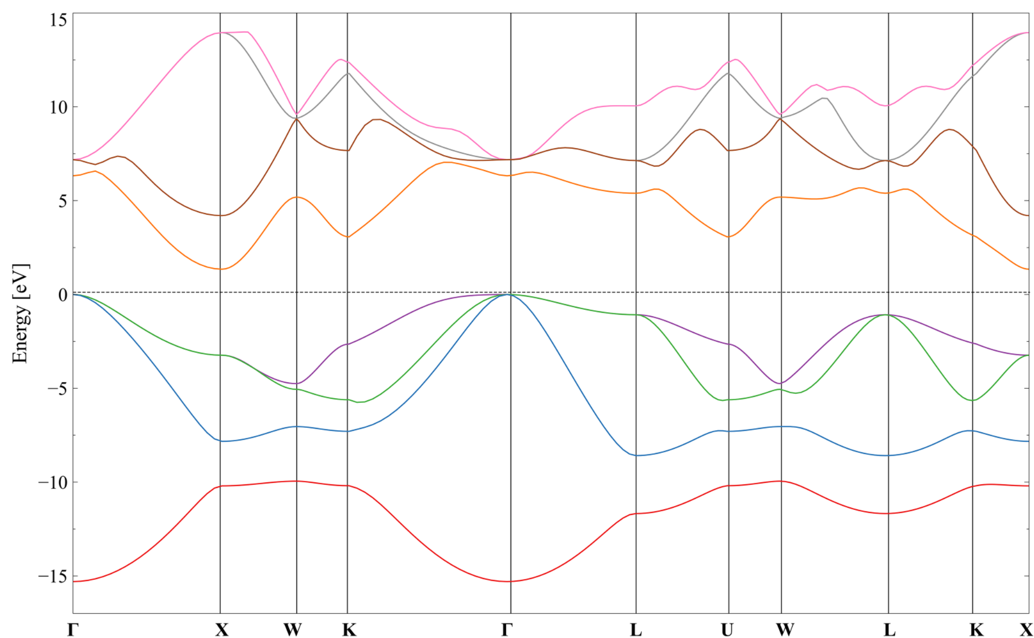

FIG. 4. Electron band structure of pristine 3C-SiC. Zero energy coincides with the valence band maximum (VBM).

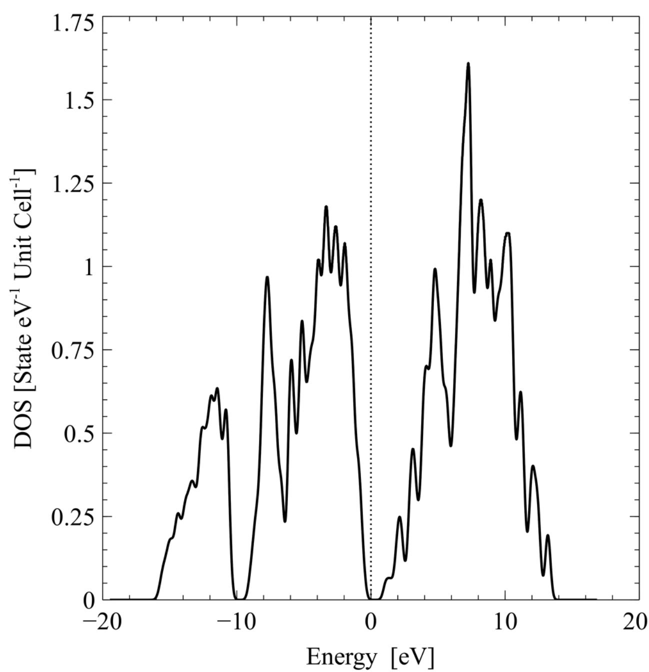

FIG. 5. Electron density of states of pristine 3C-SiC.

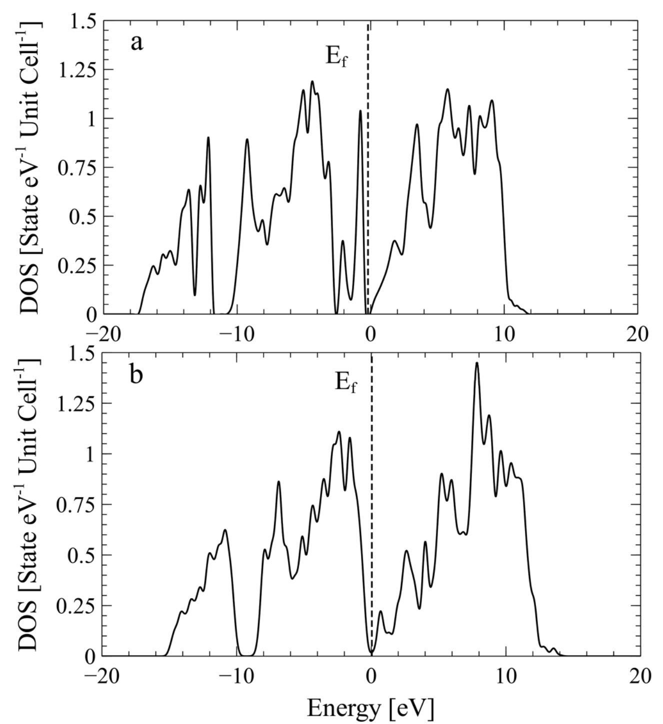

FIG. 6. (a) Electronic DOS of $Si_{0.875}C$ and (b) electronic DOS of $SiC_{0.875}$.

Published under an exclusive license by AIP Publishing

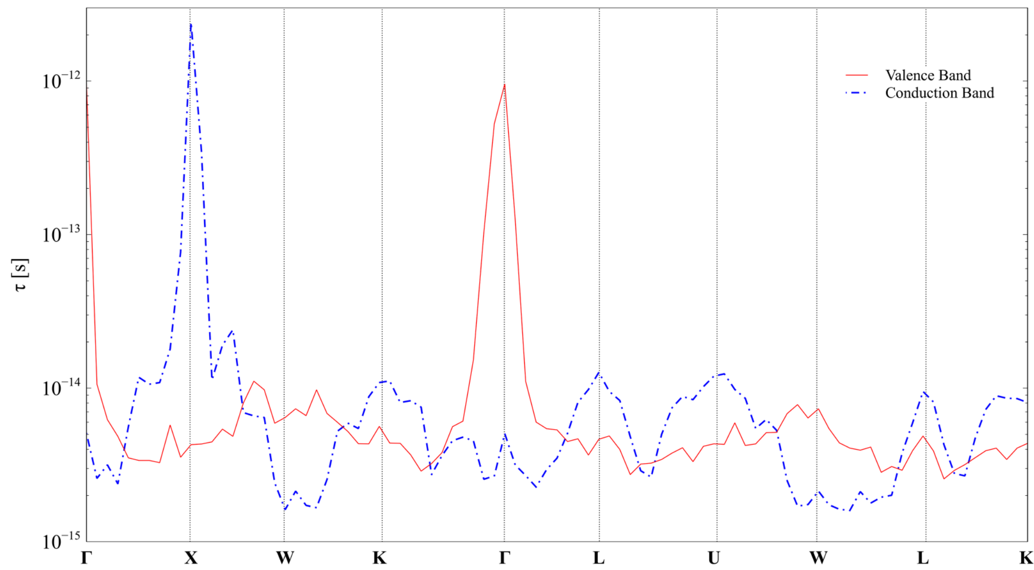

FIG. 7. Relaxation times along a Brillouin zone path calculated on a fine 46 × 46 × 46 q-grid. The uppermost valence band is shown in red. The lowest conduction band is shown in blue.

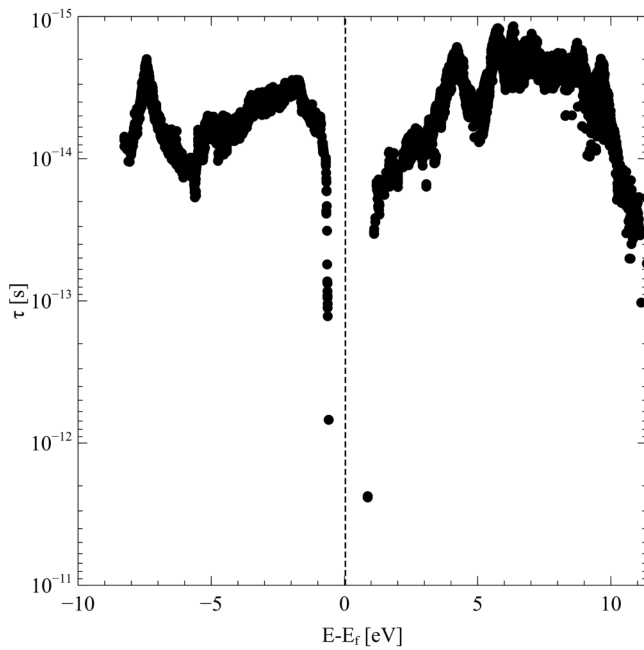

FIG. 8. Relaxation time vs the energy difference from the Fermi level for pristine 3C-SiC at 20 K.

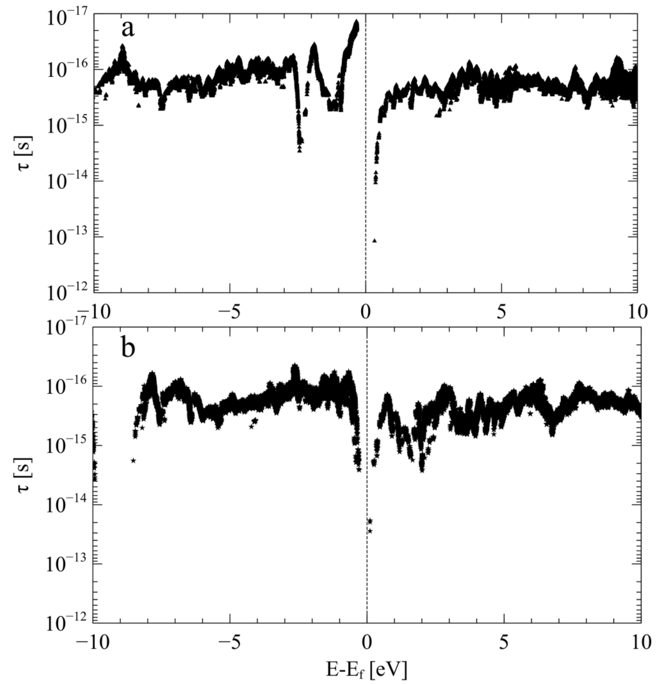

FIG. 9. (a) Relaxation time vs energy in $Si_{0.875}C$ and (b) relaxation time vs energy in $SiC_{0.875}$.

Published under an exclusive license by AIP Publishing

The electronic specific heat capacities calculated using Eqs. (6)–(9) are shown in Fig. 10. At temperatures below 10^5 K, nearly all electrons are accounted for in the static band structure calculations and $n_{free}(T) \cong 0$. At those temperatures, modification of the electronic density of states has a profound effect on the specific heat capacity. In $Si_{0.875}C$, the narrowing of the bandgap increases the density of states near the Fermi level. Those states make a greater contribution to the specific heat capacity. In $SiC_{0.875}$, the partial overlap of the bands further increases the density of states near the Fermi level. As the temperature increases, however, the broadening of the Fermi–Dirac distribution smears out the details of the band structure. Also, a larger number of electrons are treated as free electrons. Eventually, at very high temperatures, the heat capacity approaches the classical value for a Maxwell–Boltzmann gas, i.e., $c_v \cong \frac{3}{2}Nk_B$, where N is the number of valence electrons per unit volume.

Using the mode-resolved specific heat capacities and relaxation times, the electron–phonon coupling factors were calculated from Eq. (10). The coupling factors are shown in Fig. 11. In all cases, G increases as T_e increases. Over all temperatures, the vacancies increase the coupling factor by several orders of magnitude, but the increase is most pronounced at low temperatures. Interestingly, the differences in specific heat and relaxation times between the defective structures seem to largely cancel out. The larger specific heat for $SiC_{0.875}$ is compensated for by its longer relaxation time. Thus, the values of G are similar for both defective structures over all temperatures.

The electron mobilities calculated from the relaxation times are compared with the experimental electron Hall mobilities measured in lightly (unintentionally) donor-doped 3C-SiC in Fig. 12.[27] Calculated values from the Caughey–Thomas model[28] are also

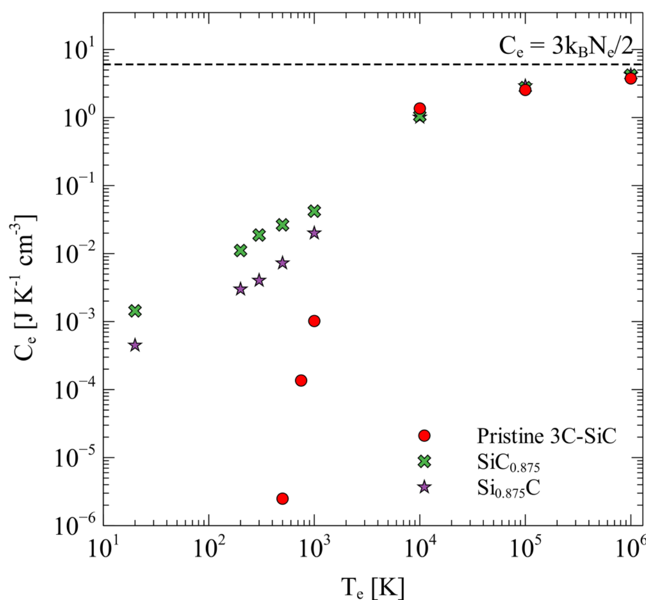

FIG. 10. Electronic specific heat capacity as a function of electron temperature.

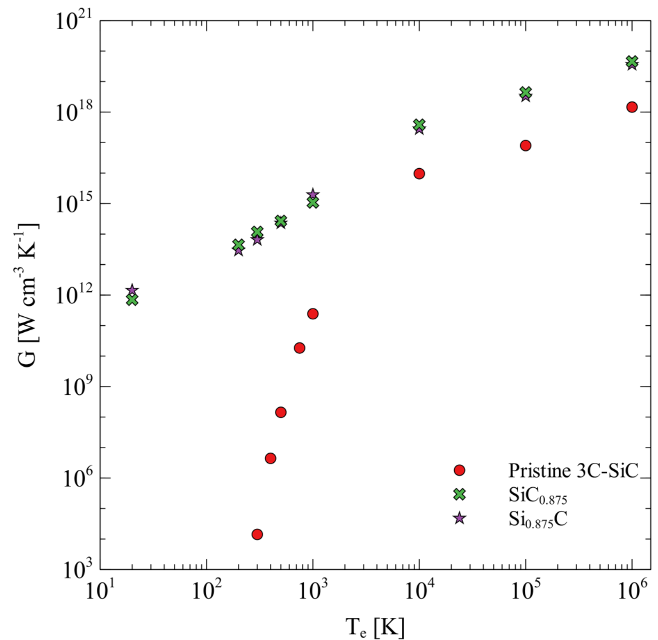

FIG. 11. Electron–phonon coupling factor vs electron temperature for pristine SiC, $SiC_{0.875}$, and $Si_{0.875}C$.

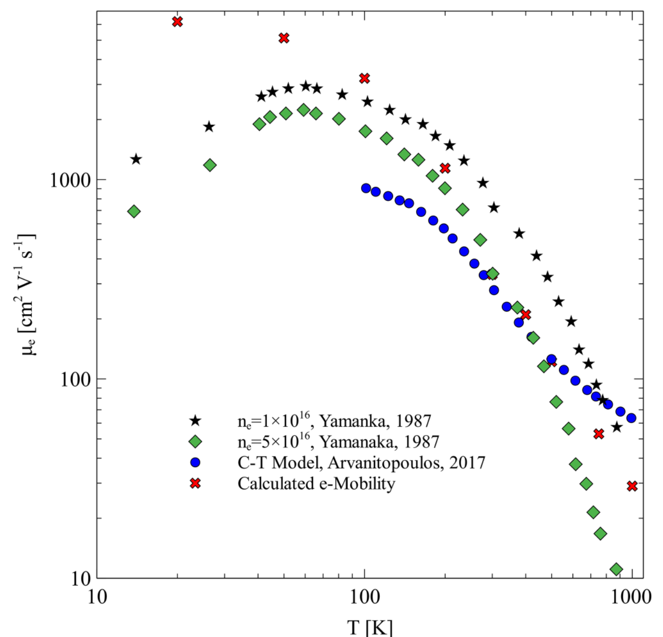

FIG. 12. Electron mobilities calculated in the present model (red crosses) along with Hall mobilities measured for lightly doped 3C-SiC taken from Ref. 27 and values calculated using the Caughey–Thomas (blue circles) taken from Ref. 28.

Published under an exclusive license by AIP Publishing

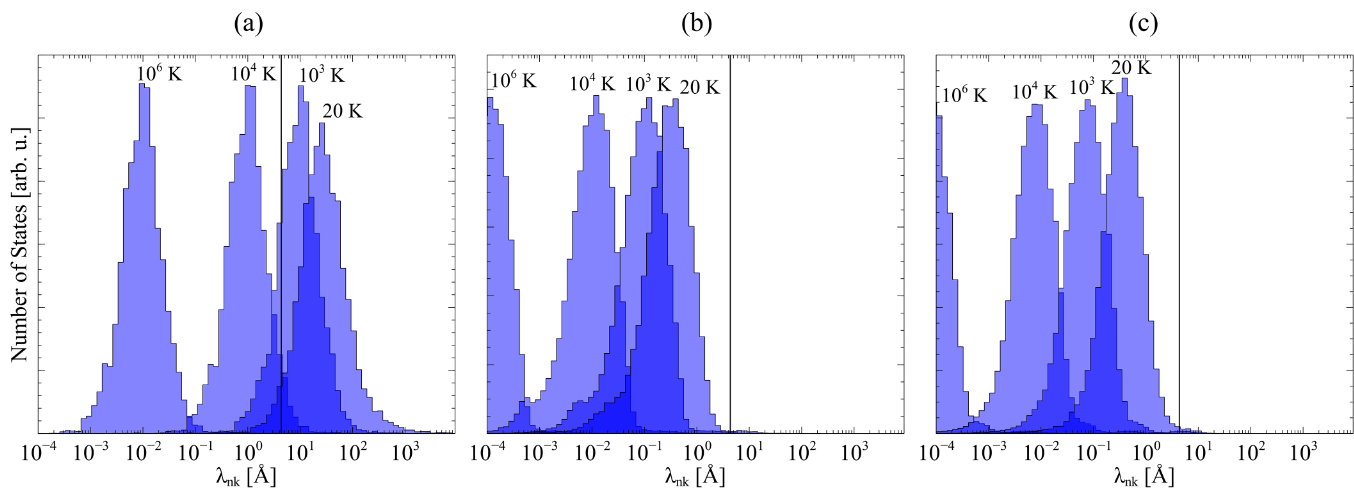

FIG. 13. The electron mean free path of (a) pristine cell, (b) $Si_{0.875}C$, and (c) $SiC_{0.875}$. The vertical line corresponds to the lattice constant.

overlaid. There is reasonably good agreement between the calculations and data when one takes into account the following factors. First, there is inherent variability in Hall measurements due to impurity concentration.[27] These calculations do not consider several relaxation mechanisms such as electron–electron scattering, electron-dislocation scattering, and electron-impurity scattering. The latter mechanism accounts for the larger differences between the calculated and measured mobilities at 20 and 50 K. As temperature decreases, the lattice scattering rate decreases while the impurity scattering rate increases.[29] The inflection in the experimental data around 60 K indicates the presence of both impurity and lattice scattering. Since the present calculations do not include the effects of impurities, the higher mobilities at 20 and 50 K are expected. Also note that in the calculations, only the electron temperature is varied. The lattice temperature is fixed at 0 K and therefore, only Stokes processes are accounted for. At elevated temperatures, the anti-Stokes processes should also reduce the electron mobility. Nevertheless, better than order of magnitude agreement was observed in a temperature range where lattice scattering (electron–phonon coupling) is the dominant relaxation mechanism.

The mean free paths of electrons calculated using Eq. (15) are shown in Fig. 13 as histograms. The main outcome from the calculation is that the mean free paths of electrons in the defective cells are smaller than the lattice parameter at temperatures greater than 200 K. This implies that when electrons scatter in the presence of vacancies, the scattering is highly localized, perhaps occurring over a length scale of an atom or a bond. This suggests that it may be possible to use a rule-of-mixtures approach in interpolating G over a range of stoichiometries given by SiC_x and Si_xC where $0.875 < x < 1.0$. Between 20 and 200 K, there are a small number of states with mean free paths larger than the lattice constant. Since some of those states can carry a significant fraction of the specific heat capacity, it may not be reasonable to use a rule-of-mixtures approach as the interaction can take place over several unit cells.

Interpolation to other stoichiometries may be further complicated by non-linearities in the DOS and band structure. Defective $2 \times 2 \times 2$ supercells, though necessary to make the problem computationally tractable, cannot be regarded as a small perturbation to the pristine cell from an isolated vacancy. Figure 6 shows a clear narrowing of the bandgap and, in the case of $SiC_{0.875}$, a semimetallic DOS. At much lower defect concentrations, localized defect states are expected to be more-or-less uncoupled and show negligible dispersion (i.e., exhibit flatbands). A $2 \times 2 \times 2$ supercell might not provide an accurate approximation of the effect of an isolated point defect on states near E_f. That said, it is clear from comparing Figs. 8 and 9 that vacancy defects have a profound effect on the lifetimes of states of all energies within the band structure. Future work will need to be conducted to (1) validate the rule-of-mixtures approximation either using larger supercell calculation or some other approximation and (2) calculate the coupling constant for various stoichiometries and explore its impact on the two-temperature model.

IV. CONCLUSION

Electron relaxation times, specific heat capacities, electron drift mobilities, electron–phonon coupling factors, and electron–phonon mean free paths were calculated for pristine 3C-SiC, $Si_{0.875}C$, and $SiC_{0.875}$ for electron temperatures from 20 to 10^6 K. The calculations were performed using a hybrid model that combines density functional perturbation theory calculations with a free electron gas model. The model was validated by comparing calculated electron mobilities with measured Hall mobilities.

Vacancy defects have a profound effect on the electron specific heat capacity at low temperatures due to changes in the electron density of states near the Fermi level. The relaxation times decrease and the electron–phonon coupling factors increase by several orders of magnitude in the defective structures compared to

Published under an exclusive license by AIP Publishing

pristine 3C-SiC. Both vacancy types have nearly the same magnitude of effect on the coupling factor. Perhaps most importantly, the coupling factor strongly depends on the electron temperature. Such temperature dependence is not usually accounted for in the two-temperature model. While an effective electron–phonon coupling *constant* has been used as a fitting parameter within the two-temperature model to successfully explain experimental data from swift heavy ion irradiations and pulsed laser experiments, the consequences of the strong temperature dependence on the coupling factor should be investigated further.

Electron–phonon mean free paths calculated in the defective supercells were found to be, in most cases, much smaller than the lattice constant. This suggests that it may be possible to interpolate the electron–phonon coupling factors to other stoichiometries of SiC using a simple rule-of-mixtures approach. This will need to be confirmed by either performing the calculations in a larger supercell, in effect lowering the vacancy concentration, or through an alternative approach.

ACKNOWLEDGMENTS

The authors thank the Information Technology teams of the Missouri University of Science and Technology and the University of Missouri-Columbia for their help and support. This work was supported in part by U.S. Nuclear Regulatory Commission Faculty Development under Grant No. NRC-HQ-84-15-G-0044. The authors have no conflicts to disclose.

DATA AVAILABILITY

The data that support the findings of this study are available from the corresponding author upon reasonable request.

REFERENCES

[1]W. J. Kim, D. Kim, and J. Y. Park, Nucl. Eng. Technol. **45**, 565 (2013).
[2]T. Wang, Z. Gui, A. Janotti, C. Ni, and P. Karandikar, Phys. Rev. Mater. **1**, 034601 (2017).
[3]Y. Katoh and L. L. Snead, J. Nucl. Mater. **526**, 151849 (2019).
[4]Z. Wang, W. E. I. Liu, and C. Wang, J. Electron. Mater. **45**, 267 (2016).
[5]S. K. Srivastava and D. K. Avasthi, Def. Sci. J. **59**, 425 (2009).
[6]J. A. Alonso and N. H. March, *Electrons in Metals and Alloys* (Academic Press, San Diego, 1989), pp. 129–203.
[7]S. Y. Savrasov and D. Y. Savrasov, Phys. Rev. B **54**, 16487 (1996).
[8]M. S. Tyagi and R. Van Overstraeten, Solid State Electron. **26**, 577 (1983).
[9]Y. Zhang, T. Varga, M. Ishimaru, P. D. Edmondson, H. Xue, P. Liu, S. Moll, F. Namavar, C. Hardiman, S. Shannon, and W. J. Weber, Nucl. Instrum. Methods Phys. Res., Sect. B **327**, 33 (2014).
[10]Q. Xu, J. Zhou, T. H. Liu, and G. Chen, Appl. Phys. Lett. **115**, 023903 (2019).
[11]M. Toulemonde, E. Paumier, and C. Dufour, Radiat. Eff. Defects Solids **126**, 201 (1993).
[12]A. Meftah, J. M. Costantini, N. Khalfaoui, S. Boudjadar, J. P. Stoquert, F. Studer, and M. Toulemonde, Nucl. Instrum. Methods Phys. Res., Sect. B **237**, 563 (2005).
[13]S. L. Daraszewicz and D. M. Duffy, Nucl. Instrum. Methods Phys. Res., Sect. B **269**, 1646 (2011).
[14]M. J. Verstraete, J. Phys.: Condens. Matter **25**, 136001 (2013).
[15]P. Ji and Y. Zhang, Phys. Lett. A **380**, 1551 (2016).
[16]M. Calandra and F. Mauri, Phys. Rev. B **76**, 205411 (2007).
[17]P. Giannozzi, O. Andreussi, T. Brumme, O. Bunau, M. Buongiorno Nardelli, M. Calandra, R. Car, C. Cavazzoni, D. Ceresoli, and M. Cococcioni, J. Phys.: Condens. Matter **29**, 465901 (2017).
[18]G. Pizzi, V. Vitale, R. Arita, S. Blüge, F. Freimuth, G. Géranton, M. Gibertini, D. Gresch, C. Johnson, and T. Koretsune, J. Phys.: Condens. Matter **32**, 165902 (2020).
[19]S. Poncé, E. R. Margine, C. Verdi, and F. Giustino, "EPW: Electron–phonon coupling, transport and superconducting properties using maximally localized Wannier functions," Comput. Phys. Commun. **209**, 116 (2016).
[20]F. Schindler, J. Geilker, W. Kwapil, W. Warta, and M. C. Schubert, J. Appl. Phys. **110**, 043722 (2011).
[21]C. Persson and U. Lindefelt, Phys. Rev. B **54**, 10257 (1996).
[22]N. Tandon, J. D. Albrecht, and L. R. Ram-Mohan, J. Appl. Phys. **118**, 045713 (2015).
[23]J. Serrano, J. Strempfer, and M. Cardona, Appl. Phys. Lett. **80**, 4360 (2002).
[24]D. W. Feldman, J. H. Parker, Jr., W. J. Choyke, and L. Patrick, Phys. Rev. **173**, 787 (1968).
[25]G. L. Zhao and D. Bagayoko, New J. Phys. **2**, 16 (2000).
[26]A. R. Lubinsky, D. E. Ellis, and G. S. Painter, Phys. Rev. B **11**, 1537 (1975).
[27]M. Yamanaka, H. Daimon, E. Sakuma, S. Misawa, and S. Yoshida, J. Appl. Phys. **61**, 599 (1987).
[28]A. Arvanitopoulos, N. Lophitis, K. N. Gyftakis, S. Perkins, and M. Antoniou, Semicond. Sci. Technol. **32**, 104009 (2017).
[29]C. Kittel, *Introduction to Solid State Physics*, 2nd ed. (John Wiley and Sons, New York, 1956), pp. 361–365.

Published under an exclusive license by AIP Publishing